An adaptive approach for texture enhancement based on a fractional differential operator with non-integer step and order

Fuyuan Hu [a,*], Shaohui Si [a], Hau San Wong [b], Baochuan Fu [a], MaoXin Si [c], Heng Luo [a]

[a] School of Electronic & Information Engineering, Suzhou University of Science and Technology, 215011, Suzhou, China
[b] Department of Computer Science, City University of Hong Kong, 999077, Hong Kong, China
[c] Jiangsu Province Software Engineering R&D Center for Modern Information Technology Application in Enterprise, 215004, Suzhou, China

ARTICLE INFO

ABSTRACT

Image texture enhancement is an important topic in computer graphics, computer vision and pattern recognition. By applying the fractional derivative to analyze texture characteristics, a new fractional differential operator mask with adaptive non-integral step and order is proposed in this paper to enhance texture images. A non-regular self-similar support region is constructed based on a local texture similarity measure, which can effectively exclude pixels with low correlation and noise. Then, through applying sub-pixel division and introducing a local linear piecewise model to estimate the gray value in between the pixels, the resulting non-integral steps can improve the characterization of self-similarity that is inherent in many image types. Moreover, with in-depth understanding of the local texture pattern distribution in the support region, adaptive selection of the fractional derivative order is also performed to deal with complex texture details. Finally, the non-regular fractional differential operator mask which incorporates adaptive non-integral step and order is constructed. Experimental results show that, for images with rich texture contents, the effective characterization of the degree of self-similarity in the texture patterns based on our proposed approach leads to improved image enhancement results when compared with conventional approaches.

© 2014 Elsevier B.V. All rights reserved.

1. Introduction

Image texture enhancement aims to improve the quality of an image by modifying its attributes. A number of cutting-edge techniques have been proposed which can be divided into two categories: transform-based [1] and spatial domain-based [2]. Transform-based methods regulate coefficients associated with the frequency domain, followed by an inverse transform to obtain the resulting image, based on which image enhancement can be achieved. However, these methods may introduce ringing effect and additional noise. On the other hand, spatial domain-based methods can avoid these problems without the need to perform frequency domain transform, resulting in less computation. Among the different enhancement approaches, the differential mask operator stands out as a particularly important example. Differential operator masks can be further categorized as integral differential and fractional differential operators. As for image improvement, most integral-differential operators (e.g., Sobel, Prewitt, and Laplacian of Gaussian operators) behave well when used for enhancing high-frequency features. Nevertheless, their performance deteriorates significantly when applied to smooth regions.

Pu et al. [3] apply the theory of fractional differential operator to address these problems. Since a fractional differential operator is capable of characterizing fractal-like structures [4] which are often found in the texture regions, this class of operator is considered as an effective tool for texture enhancement in images. Through analyzing the geometric and physical properties of fractional differential operators, Pu et al. [3] have developed an $n \times n$ fractional differential operator mask, and it was noticed that the adoption of the mask results in better enhancement of texture details compared to traditional integral-based differential operators [5]. It was further observed that the fractional differential operator has the capability of not only preserving high-frequency contour features, but enhancing the low-frequency texture details in smooth areas as well. Gao et al. [6] applied the fractional differential operator to quaternions, and designed a set of masks which are referred to as quaternion fractional differential (QFD) operators, which generalize the previous fractional differential operators.

However, for image enhancement, some problems still exist with the fractional differential operator. To begin with, traditional fractional differential operators usually consider fixed-size mask templates, leading to ineffective processing of pixels corrupted by noise and with low correlations. Moreover, the spatial step in the numerical implementation of the fractional differential operator based on the definition of Grümwal–Letnikov usually advances by one. In other words, the default minimum distance is assumed to be one pixel. As a result, the high degree of self-similarity that many images exhibit is not well characterized. In addition, it is not

convenient to manually search for the optimal fixed fractional derivative order which matches the local texture details. In view of these problems, we propose a novel fractional differential operator mask with adaptive non-integral step and order in this paper for the enhancement of texture details. The main contributions of this paper are as follows:

(1) We identify local non-regular self-similar support regions by analyzing texture features, such that highly correlated pixels can be focused on while noisy pixels are excluded.
(2) We select non-integral steps and fractional orders for the support region in an adaptive way, such that the degree of self-similarity in complex textures can be well characterized.
(3) We design a non-regular fractional differential operator mask with fractional order and adaptive non-integral steps, such that the texture enhancement performance can be optimized regardless of whether the regions consist of high or low frequency patterns.

The paper is organized as follows. The proposed algorithm is introduced in Section 2, followed by the analysis of experimental results in Section 3. Finally, our conclusions are summarized in Section 4.

2. Fractional differential operator mask with adaptive non-integral step and order

As complex textures are characterized by irregular and disorderly patterns, a novel approach based on adaptive fractional differential operator is proposed in this paper to enhance these patterns. Fig. 1

provides an overview of the algorithm. As can be seen, with a suitable texture similarity measure, a local support cross skeleton domain, i.e. $\{h_p^i\}$, where $i \in \{0, 1, 2, 3\}$ denotes the four directions, can be defined. Once such a support skeleton domain, which can be partitioned into two sets $H(p)$ and $V(p)$ corresponding to the horizontal and vertical directions respectively, is determined, a non-regular support region $\Omega_p = \cup_{q \in V(p)} H(q)$ can be constructed. Based on the proposed skeleton domain and its associated support region, the local adaptive fractional order can be dynamically determined, and the result can be computed at a sub-pixel resolution.

2.1. Non-regular support region with self-similarity

Before introducing the non-regular support region, we first define the following notations. As shown in Fig. 2(c), Ω_p is defined as the non-regular neighboring region of an anchor point p. W_p is a square window of radius r which represents the traditional fixed size mask.

Unlike [7] where the pixel value I_p is used as the reference value, we update it dynamically based on a weighted combination of itself and neighboring pixels at a distance h, which makes the skeleton more robust against noise. Considering the right arm h_p^0 of the skeleton for p, the updated reference value is given as

$$\tilde{I}_p^{(h_p^0)} = (1-\alpha)\tilde{I}_p^{(h_p^0 - 1)} + \alpha I(x + h_p^0, y) \qquad (1)$$

where $\tilde{I}_p^0 = I_p$, and α is a parameter for controlling the pixel similarity and update rate. Limited by the support radius of W_p, the right span h_p^0 is within the range $[1, r]$. In our case, h_p^0 corresponds to the value of a parameter m ($m \in [1, 2, \cdots, r]$), such that the
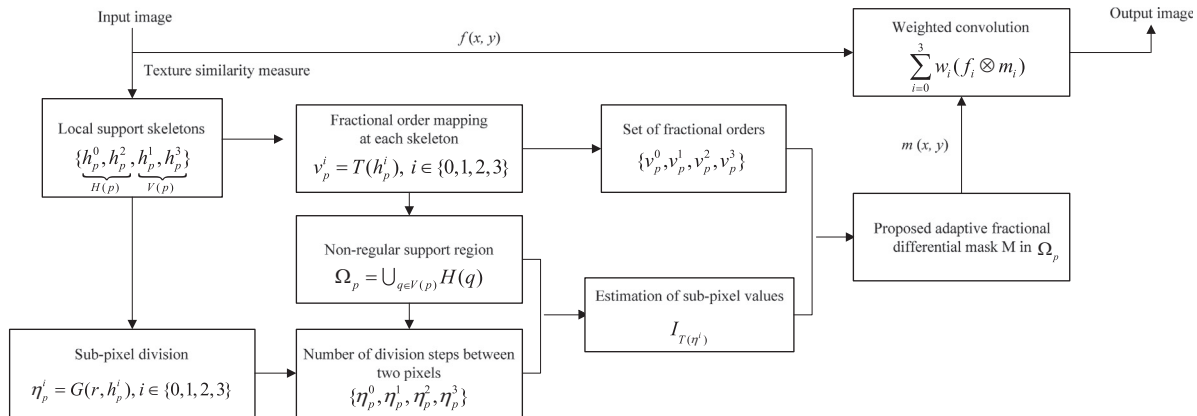

Fig. 1. Block diagram of the proposed method.
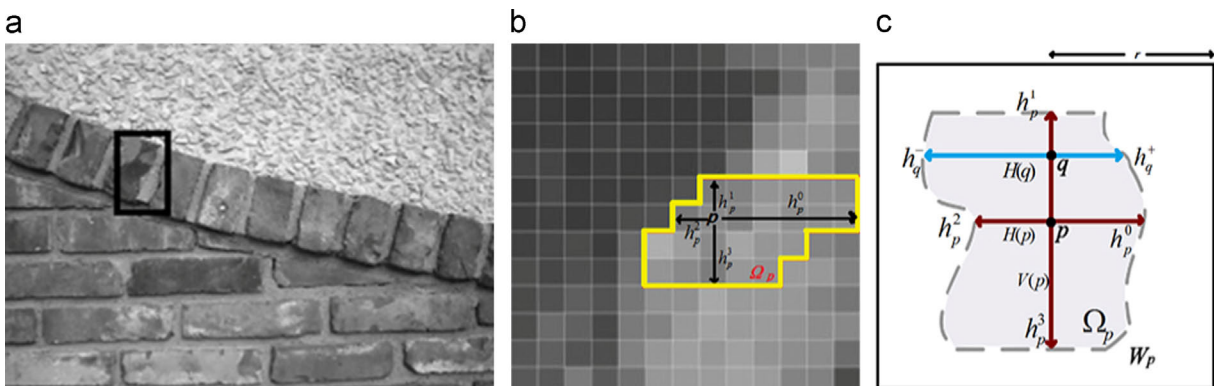

Fig. 2. Local non-regular support region construction: (a) original image, (b) local support region corresponding to the black box in (a), and (c) model of the support region.

condition $\left|I(x+m,y)\right|-\left|\tilde{I}_p^{(m-1)}\right| > \tau$ is satisfied, where τ is a similarity threshold. The values of $\left\{h_p^1, h_p^2, h_p^3\right\}$ can be obtained in a similar way.

For a pixel q, where $q \in V(p)$, the optimal values of the horizontal directional spans $\{h_q^+, h_q^-\}$, as shown in Fig. 2(c), are obtained in a similar way as those of $\left\{h_p^0, h_p^2\right\}$. Therefore, the non-regular support region Ω_p with self-similarity is denoted as

$$\Omega_p = \cup_{q \in V(p)} H(q) \tag{2}$$

2.2. Dynamic estimation of sub-pixel values

In view of the high degree of self-similarity in images, the pixel values are closely related to the arm lengths along different directions within the support region. The values tend to be similar along directions with longer arm lengths, while they change more frequently along directions with shorter arm lengths. In other words, the self-similarity of neighboring pixels will increase with h_p^i. When h_p^i is large enough, the correlation of the pixel values can be effectively estimated through an integral number of pixels, and no
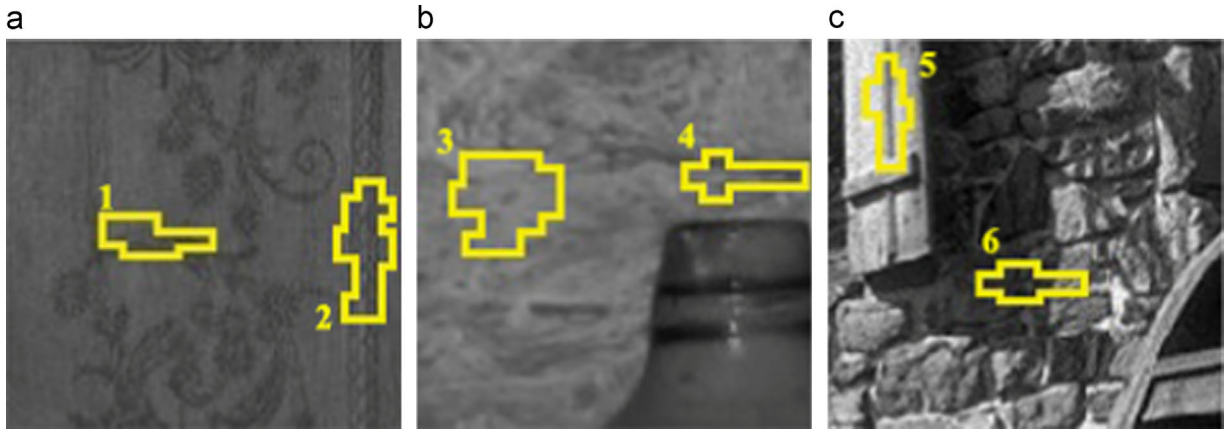

Fig. 3. Non-regular support regions in smooth areas: (a) table linen, (b) wall, and (c) stone house. (For interpretation of the references to color in this figure, the reader is referred to the web version of this article.)
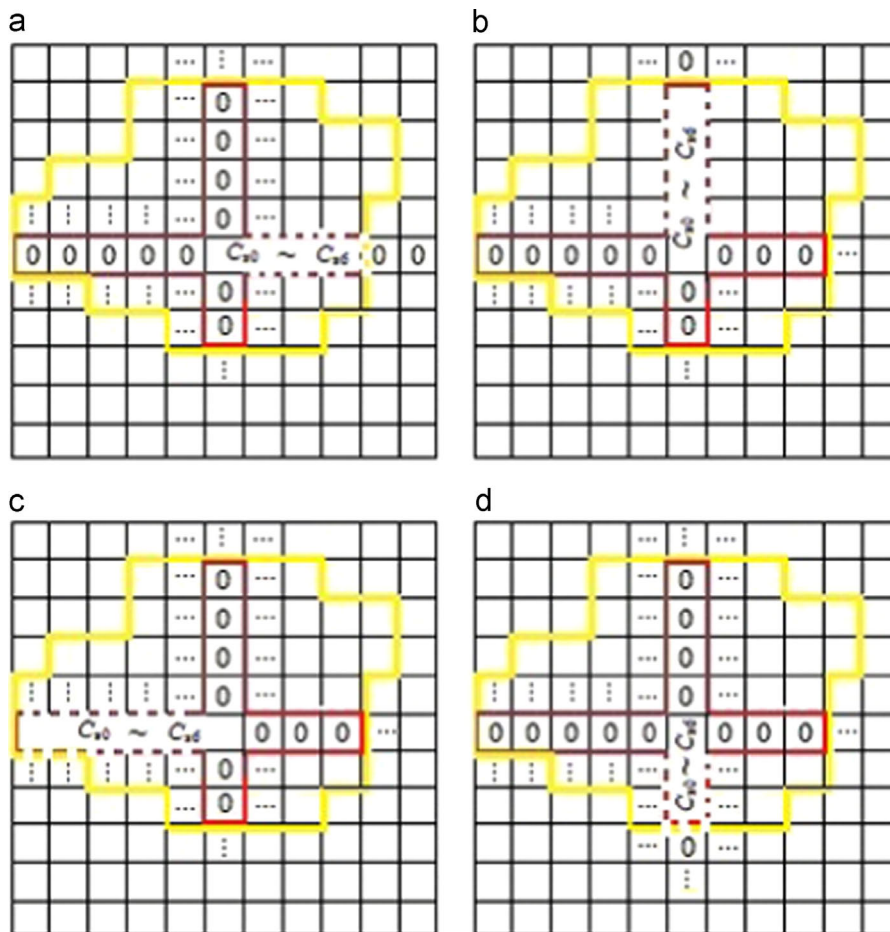

Fig. 4. Fractional differential operator mask along four directions: (a) h^0, (b) h^1, (c) h^2, and (d) h^3.

further sub-division of the pixels is necessary. On the other hand, a small value of h_p^i may lead to an underestimation of the degree of self-similarity. As a result, it is necessary to sub-divide the original set of pixels into sub-pixels when the directional arm h_p^i is small as follows:

$$\eta_p^i = G(r, \ h_p^i) = \left\lfloor \frac{r}{N(h_p^i) + \xi_p^i} \right\rfloor, \quad h_p^i \in \left\{ h_p^0, \ h_p^1, \ h_p^2, \ h_p^3 \right\} \quad (3)$$

where η_p^i denotes the number of sub-pixels to be generated between two original pixels, $\lfloor \ \rfloor$ is the floor operator, $N(h_p^i)$ represents the number of integral pixels that one of the arms covers, and ξ_p^i is a pre-specified parameter.

With a suitable choice of ξ_p^i, we limit the value of η_p^i to the range [0, 2]. A value of $\eta_p^i = 0$ indicates that there is no need to divide the unit pixel interval. We average the neighboring integral pixels along the arm direction when $\eta_p^i = 1$. On the other hand, when $\eta_p^i = 2$, a local piecewise linear model is adopted to estimate the intensity of the sub-pixels, which is given as

$$I_k = a_1^k Y + a_2^k, \quad \eta_p^i = 2 \quad (4)$$

where $k = m + \frac{1}{\eta_p^i + 1} \cdot c$ represents the location of a sub-pixel, and $c \in \{1,2\}$ corresponds to the c-th interval, a_1^k and a_2^k are model

parameters, and Y denotes a reference integral pixel gray value which is either I_m or I_{m+1}, depending on which one is closer to the current sub-pixel along the arm direction.

2.3. Adaptive selection mechanism for the fractional order

Examples of non-regular support regions are highlighted in yellow in Fig. 3. As can be seen, the arm lengths of regions 1, 4 and 6 are longer along the horizontal direction, and shorter along the vertical direction. On the other hand, regions 2 and 5 have longer arm lengths along the vertical direction. Since the arm lengths reflect the dominant direction of the underlying texture patterns, we aim to enhance the texture along these major directions, and attenuate the pattern along the minor directions. This can be achieved by increasing the fractional order for the longer arms, and decreasing the order for the shorter arms.

As observed in [3], a suitable range of the fractional order v is from 0.4 to 0.7. To design a smooth mapping between h_p^i and v_p^i, we consider the following exponential model:

$$v_p^i = T(h_p^i) = b_1 \exp\left(-\frac{h_p^i}{r}\right) + b_2, \quad h_p^i \in [1, \ r] \quad (5)$$
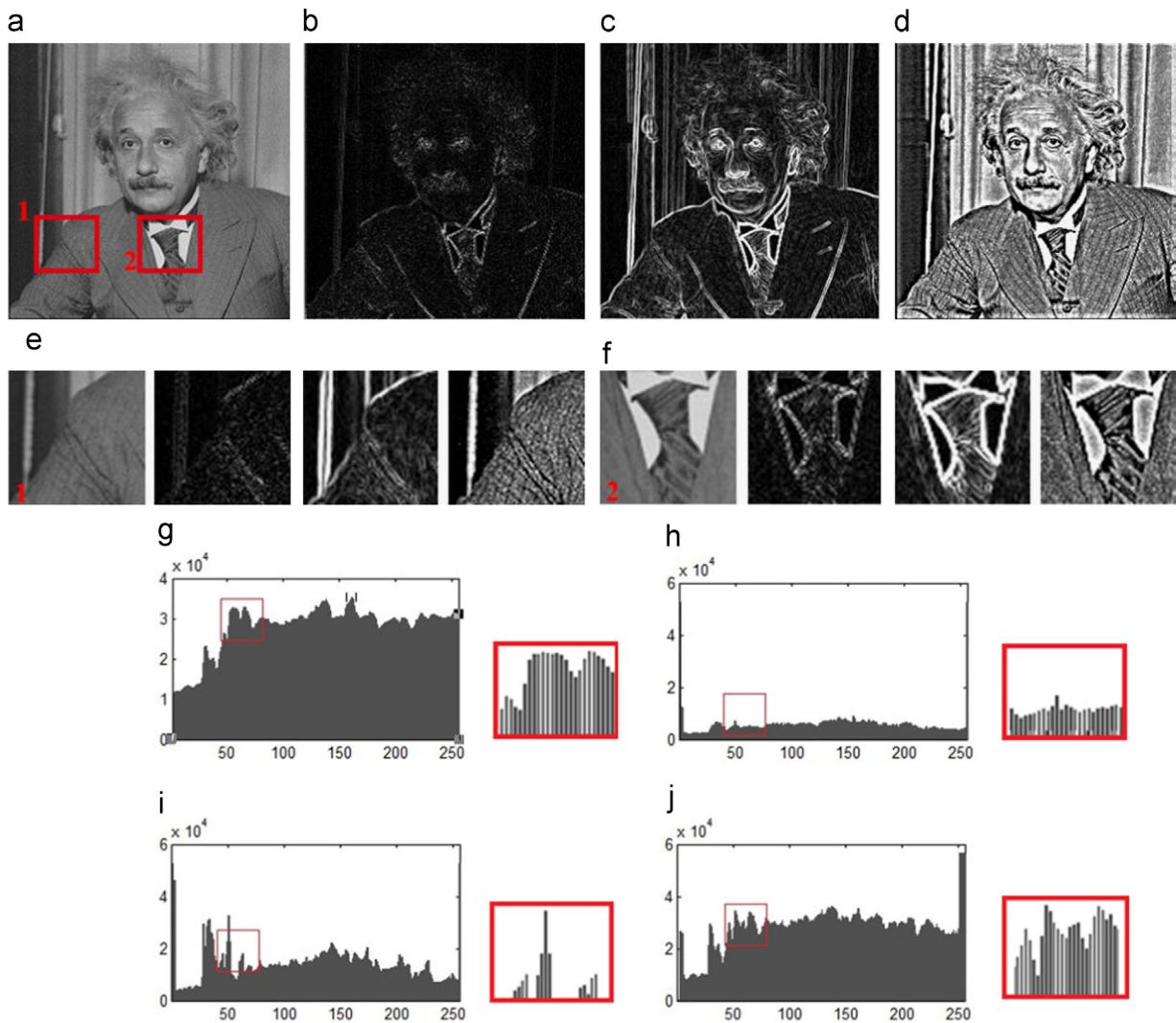

Fig. 5. Comparison between integral differential operators and our operator: (a) original, (b) Laplacian, (c) Sobel, and (d) our result. The local texture highlighted in red is enlarged in (e) and (f), and their corresponding vertical projections are shown in (g)–(j) respectively. (For interpretation of the references to color in this figure legend, the reader is referred to the web version of this article.)

where b_1 and b_2 are model parameters. In addition, v_p^i should meet the following requirements:

$$\begin{cases} v_p^i \in [\beta_1, \beta_2] \\ \beta_1, \beta_2 \in [0.4, 0.7] \\ v_p^i = \beta_1|_{h_p^i = r}, \quad v_p^i = \beta_2|_{h_p^i = 1} \end{cases} \quad (6)$$

Based on Eq. (5), the set of fractional orders $\{v_p{}^0, v_p{}^1, v_p{}^2, v_p{}^3\}$ can be computed.

2.4. Adaptive fractional differential operator mask construction

Due to different texture pattern distribution and degree of self-similarity along the four directions, each arm has its own fractional order and non-integral step. Therefore, the approximate
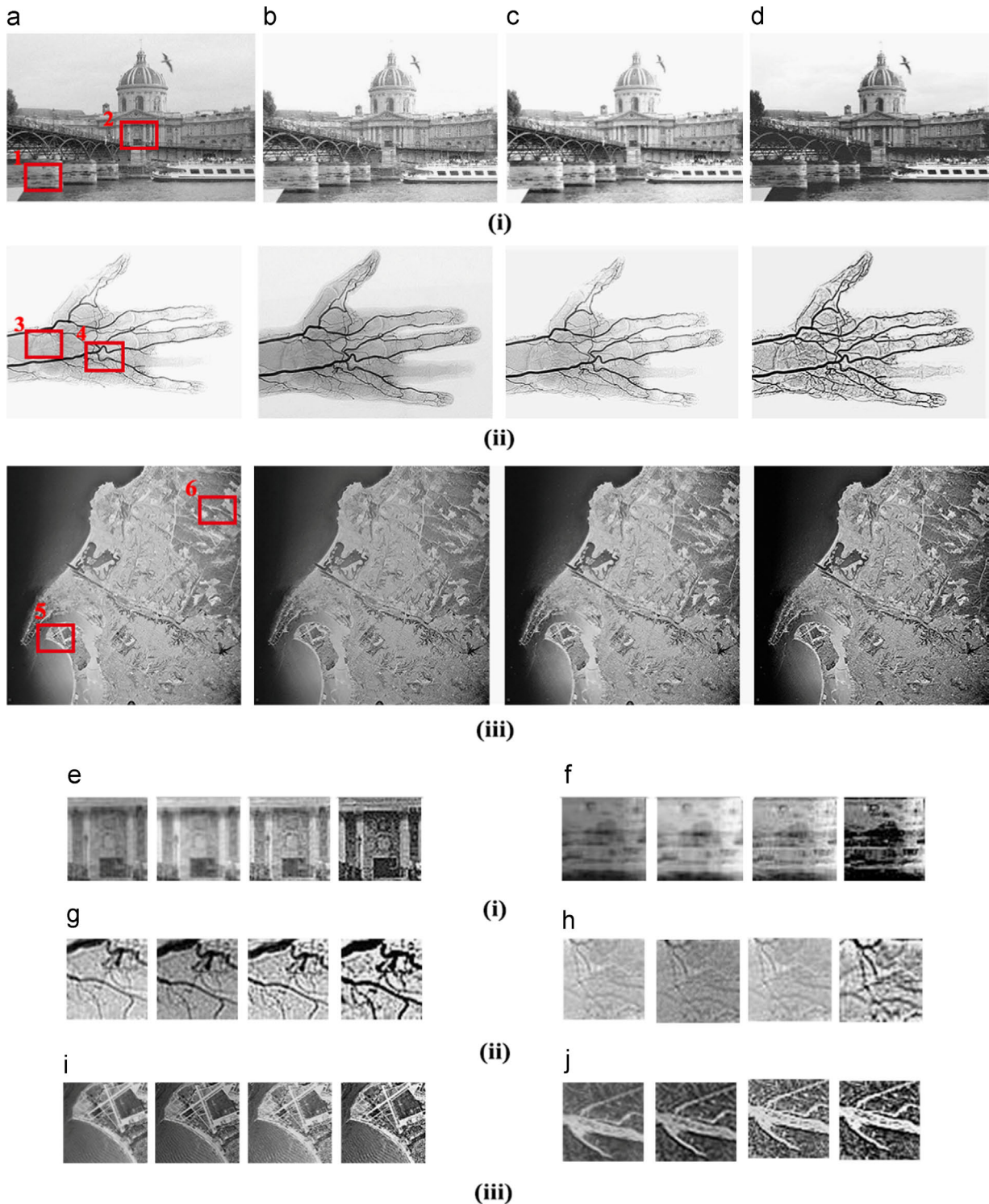

Fig. 6. Results of different fractional differential operator methods. Three test images are selected: (i) bridge, (ii) hand (X-ray), and (iii) channel (remote sensing). (a) Original, (b) R–L, (c) Pu's result, and (d) our result. The local regions highlighted in red are enlarged in (e)–(j). (For interpretation of the references to color in this figure legend, the reader is referred to the web version of this article.)

form of the fractional derivative of a signal $f(t)$ can be expressed as

$$\frac{d^v f(t)}{dt^v} \approx \frac{1}{(\eta_p^i+1)^{v_p^i}} \sum_{m=0}^{t-a} \sum_{c=0}^{\eta_p^i} \begin{bmatrix} v_p^i \\ m \\ \eta_p^i \end{bmatrix} f\left[t-\left(m+\frac{1}{\eta_p^i+1}\cdot c\right)\right] \quad (7)$$

Table 1
Evaluation results (AG, AE, and APSNR) of different fractional differential operator methods.

Images	Evaluation	R–L	Pu's result	Our result
Building	AG	0.0325	0.0461	0.1211
	AE	7.1102	7.0914	7.5209
	APSNR	13.0211	14.4533	18.1760
Hand (X-ray)	AG	0.0598	0.0671	0.0973
	AE	5.8670	4.0678	5.978
	APSNR	16.1891	17.4944	20.9798
Channel (remote sensing)	AG	0.0278	0.0644	0.0767
	AE	7.4953	7.5451	8.1062
	APSNR	15.5417	16.8505	19.4330

where a denotes the interval within which the numerical derivative is evaluated, $\begin{bmatrix} v_p^i \\ m \\ \eta_p^i \end{bmatrix} = \frac{(-1)^{m\cdot(\eta_p^i+1)+c}\Gamma(-v_p^i+1)}{[m\cdot(\eta_p^i+1)+c]!\Gamma\{-v_p^i-[m\cdot(\eta_p^i+1)+c]\}}$, and Γ denotes the gamma function.

To ensure that the fractional differential operator mask can sufficiently cover the spatial extent of local texture patterns, we set the value of the radius r to 5. Using this value in Eq. (3), we can dynamically compute the number of divisions between pixels. As a result, the maximum number of mask coefficients C_{s_n} along each direction is 7, and they can be computed from Eq. (7) as follows:

$$\begin{cases} C_{s_0} = \frac{1}{(\eta_p^i+1)^{v_p^i}} \times 1 \\ C_{s_1} = \frac{1}{(\eta_p^i+1)^{v_p^i}} \times (-v_p^i) \\ \vdots \\ C_{s_n} = \frac{1}{(\eta_p^i+1)^{v_p^i}} \times \frac{(-1)^n \Gamma(v_p^i+1)}{n!\Gamma(v_p^i-n+1)} \\ \vdots \\ C_{s_6} = \frac{1}{(\eta_p^i+1)^{v_p^i}} \times \frac{(v_p^i)!}{6!(v_p^i-6)!} \end{cases} \quad (8)$$
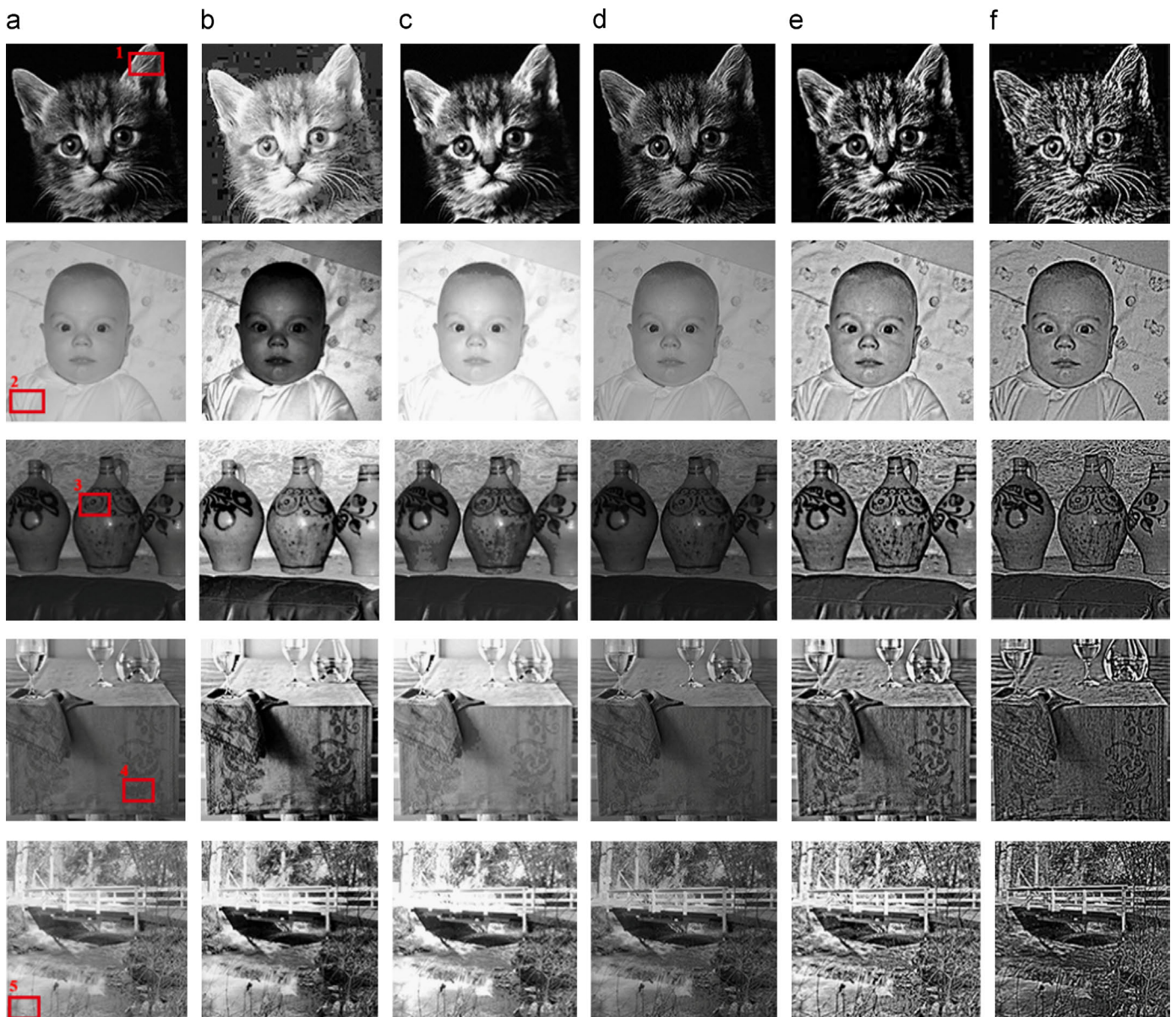

Fig. 7. More comparison with our approach: (a) original, (b) HE, (c) Xiang's result, (d) Tanaka's result, (e) GF, and (f) our result. (For interpretation of the references to color in this figure, the reader is referred to the web version of this article.)
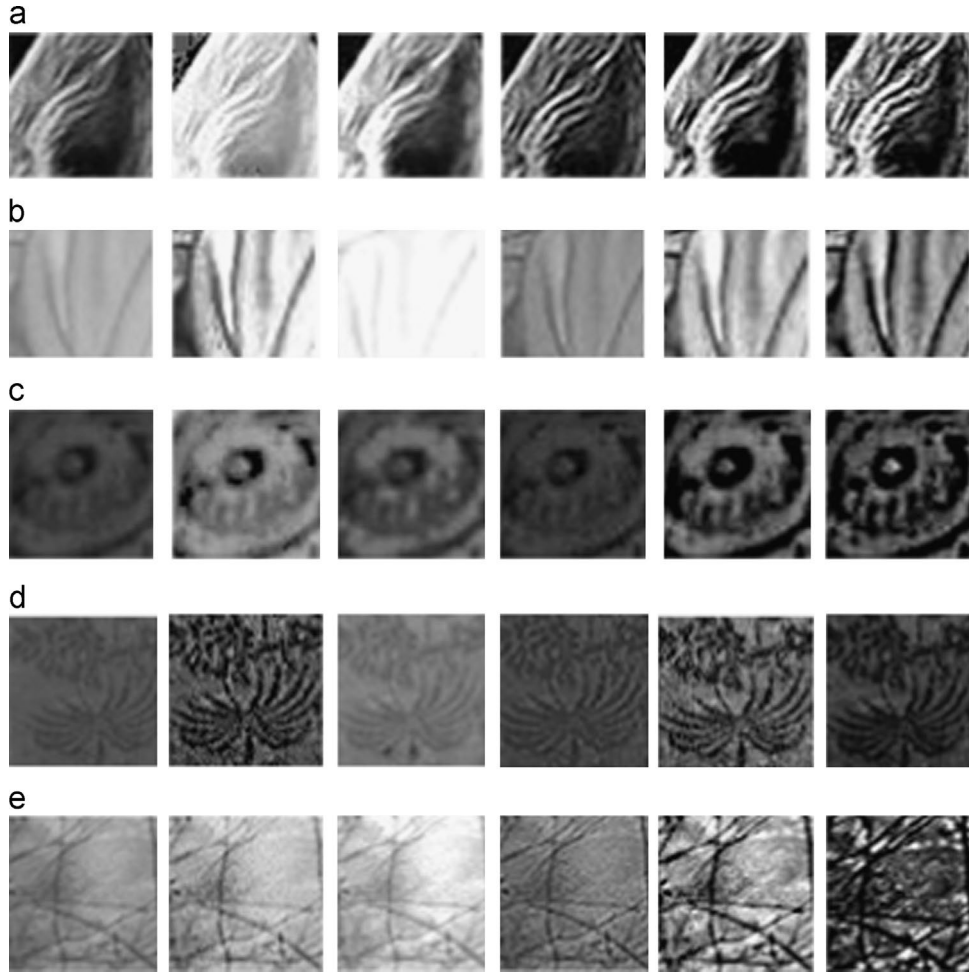
Fig. 8. Local texture detail enlargement of highlighted red regions in Fig. 7: (a) Cat's wrinkle, (b) Baby's clothes, and (c) Porcelain ware's pattern.

Table 2
Evaluation results (AG, AE, and APSNR) of different enhancement methods.

Images	Evaluation	HE	Xiang's result	Tanaka's result	GF	Our result
Cat	AG	0.0765	0.0872	0.0903	0.1265	0.1582
	AE	6.0165	6.4481	6.3183	8.7136	10.4003
	APSNR	9.2294	18.4164	19.5639	25.5906	27.9560
Baby	AG	0.0315	0.0148	0.0614	0.0412	0.0616
	AE	6.3418	4.5472	6.4432	7.2111	7.3767
	APSNR	12.5655	11.7318	17.7602	20.0147	22.7311
Porcelains	AG	0.0106	0.0123	0.0200	0.0265	0.0274
	AE	6.1004	6.5716	6.7752	7.5937	7.8716
	APSNR	10.5356	17.0059	20.1065	20.1065	24.8011
Table linen	AG	0.0408	0.0270	0.0320	0.0679	0.0825
	AE	6.7514	5.9417	6.8891	7.5855	7.6544
	APSNR	14.6699	14.6699	17.8987	21.3929	22.4762
Bridge	AG	0.0495	0.0449	0.0492	0.0501	0.1575
	AE	6.8922	6.4513	6.5728	6.9100	7.4600
	APSNR	13.8538	19.1534	19.4240	19.7488	19.7756

As a result, the operator masks corresponding to the four directions can be constructed as shown in Fig. 4. As can be seen, the highlighted yellow region is the local shape-adaptive region Ω_p, and the red region is its support cross skeleton domain. Pseudo-code for the proposed method is summarized in Algorithm 1. To achieve a balance between stability and adaptivity in the pixel update process, the parameter α is set to a suitable value

(e.g., 0.6). The similarity threshold τ can be used to determine the form of the non-regular region, and our experimental results indicate that choosing $\tau = 10$ results in better performance.

3. Experiments and analysis

We use the measures average gradient (AG) [8], average information entropy (AE) [9], and average peak signal to noise ratio (APSNR) to evaluate the performance of the proposed approach.

AG is a measure of image contrast, and larger values correspond to stronger texture patterns. The measure is defined as follows:

$$AG = \frac{1}{(M-1)(N-1)} \sum_{x=1}^{M-1} \sum_{y=1}^{N-1} \sqrt{\frac{(g_{x,y} - g_{x+1,y})^2 + (g_{x,y} - g_{x,y+1})^2}{2}} \quad (9)$$

where g denotes intensity level, and $M \times N$ is the size of an image.

Algorithm 1 : Fractional Differential Operator Mask with Adaptive Non-integral Step and Order

Input: input image f, radius r, parameter α, similarity threshold τ, parameter ξ.
Output: output image g
For each pixel
1: Use Eq. (1) to compute the local support skeleton $\{h_p^0, h_p^1, h_p^2, h_p^3\}$;
2: Use Eq. (2) to determine the non-regular support region Ω_p;
3: Use Eq. (3) to generate sub-pixels for each arm h_p^i, and Eq. (4) to compute gray values for sub-pixels;

4: Use Eq.(5) to estimate the set of fractional orders $\{v_p^0, v_p^1, v_p^2, v_p^3\}$;
5: Use Eq. (8) to compute coefficients for the mask;
6: Apply weighted convolution to obtain g.
End For

AE is a measure of the richness of image details. Smaller values indicate that less information content is associated with the image.

It is defined as follows:

$$AE = -\sum_{i=0}^{L-1} P(g_i)\log_2 P(g_i) \tag{10}$$

where $P(g_i)$ is the probability distribution function of the image intensity level g_i, and L is the total number of intensity levels.

APSNR is a standard image fidelity measure, and a higher value of APSNR indicates better performance of noise resistance.
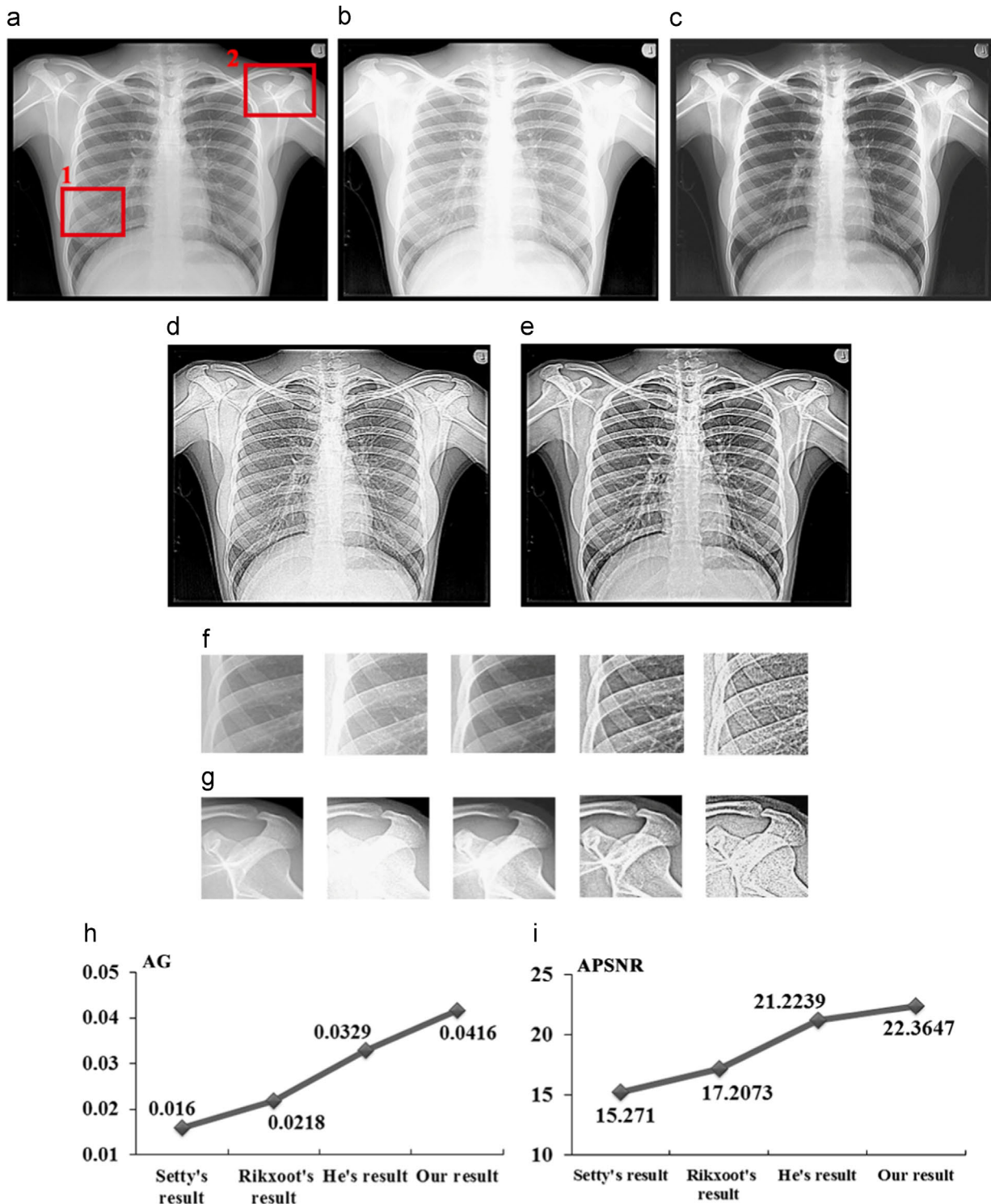

Fig. 9. The X-ray image of human chest: (a) original, (b) Setty's result, (c) Rikxoot's result, (d) GF, (e) our result, (f) and (g) enlargement of the two highlighted regions in (a), (h) evaluation results based on AG, and (i) evaluation results based on APSNR.

3.1. Comparison with integral differential operator masks

Most typical differential operator masks such as the first-order Sobel, Prewitt and Roberts operators, and the second-order Laplacian operator, are in fact integral differential operators. They may perform well in the high frequency regions, but their performance will deteriorate when applied to rich texture patterns in smooth regions. Fig. 5 shows an example which compares our approach with classical integral differential operators. The vertical projections of the image gray level values are also shown.

The results of the Laplacian and Sobel operators are shown in Fig. 5(b) and (c). The results clearly show that the rich texture in smooth areas (see Fig. 5(b) and (c), black lines on the suit, gray-black stripes on the tie) is basically removed, and the gray values of the corresponding pixels appear dark. At the same time, due to excessive enhancement of the high frequency components, wide white edges appear in those regions (see Fig. 5(e) and (f)). Different from the integral differential operators, the proposed approach takes into consideration these texture details in smooth areas, and judiciously emphasizes the local texture similarity. As a result, texture detail in the smooth regions is more distinct in Fig. 5(d). In general, the proposed algorithm outperforms the traditional integral differential operator methods on the edges in terms of its capability to avoid overly emphasizing the high frequency components (see Fig.5(f)).

The same conclusion can also be obtained from their vertical projections. It can be seen in Fig. 5(g)–(j) that the projection envelopes for the original image and the enhanced image based on our approach are highly similar, and additional peaks are added to the projection envelope of the enhanced image in our case (see the highlighted red region in Fig. 5(j)). This indicates that some of the image details have been judiciously enhanced without distorting the overall image structure. However, the projection envelopes of Laplacian or Sobel (see Fig. 5(h)-(i)) operators are very different from that of the original image, which indicates that significant image distortion has been introduced.

3.2. Comparison with other fractional differential operator approaches

Fractional differential operator methods are capable of preserving texture detail in smooth areas. However, previous methods do not take into consideration the high degree of self-similarity in images, and thus usually ignore local texture features. The performance of the proposed algorithm is compared with Pu et al., [5] and the traditional Riemann–Liouville (R–L) method in Fig. 6.

As shown in Fig. 6, while the texture details in the smooth areas are well enhanced by the R–L method in all cases, the overall brightness of the images decreases. Fig. 6(c) shows the enhancement results based on the *YiFeiPU*-2 fractional differential operator mask proposed in [5]. In spite of higher efficiency and better convergence rate, this method cannot effectively take into consideration the complexity and diversity of local texture patterns, thus leading to only
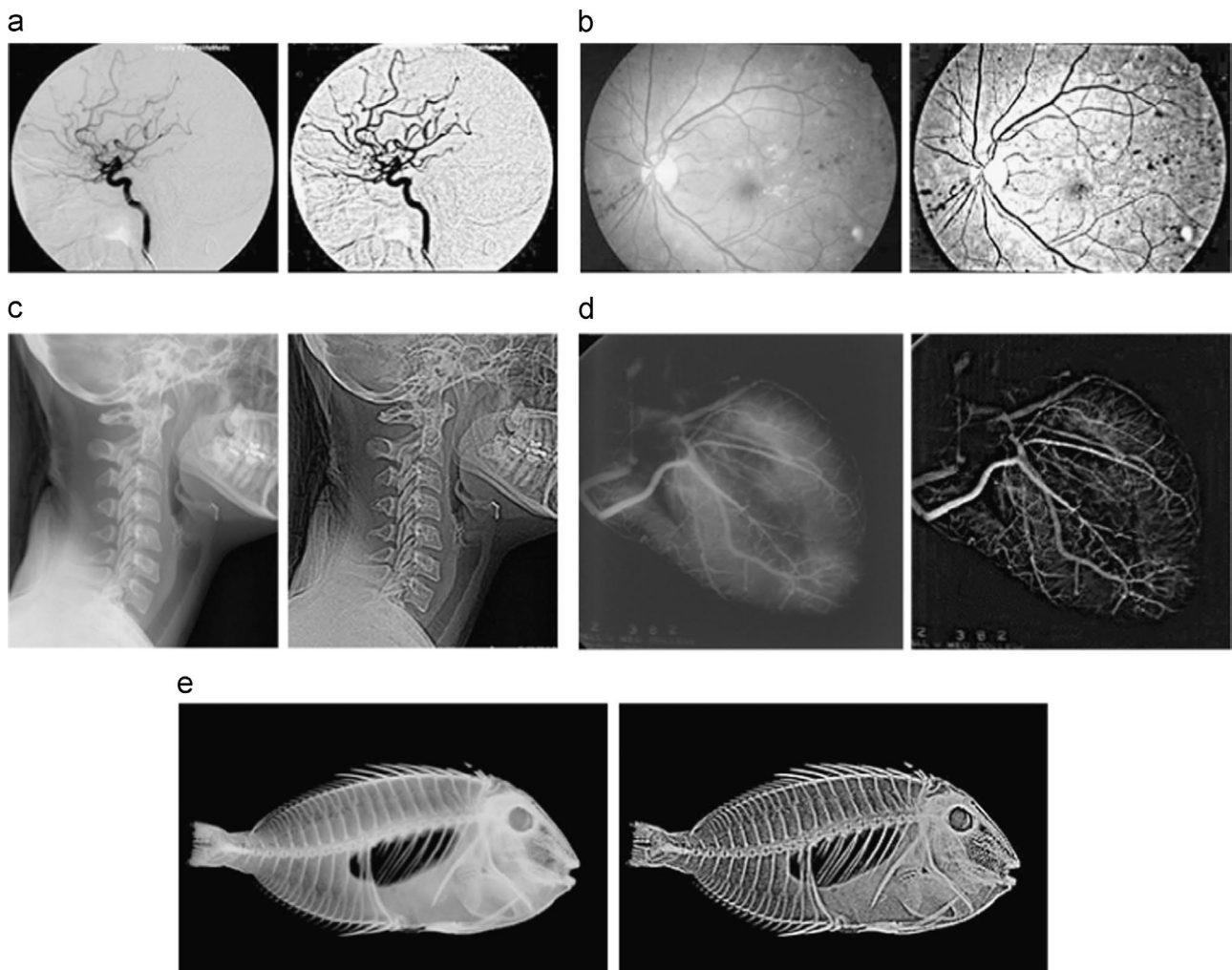

Fig. 10. Other X-ray/medical image enhancement results (left: original, right: our result): (a) cranial nerve, (b) retina, (c) vertebral column, (d) heart, and (e) fish.

marginal enhancement of the small blood vessels in Fig. 6(g) and (h). Compared with Pu's work, our approach improves the self-correlation in images and therefore it can enhance the local complex texture patterns adaptively. As can be observed, the curved patterns of the building in Fig. 6(e) and the branches of the river captured by a remote sensing satellite in Fig. 6(j) are brighter and more distinct. Table1 summarizes the performance of the proposed algorithm in terms of APSNR, AG, and AE. It is obvious that our approach suppresses noise while preserving texture details at the same time.

3.3. Comparison with different image enhancement methods

3.3.1. Image enhancement results

The proposed algorithm is compared with other popular enhancement algorithms like histogram equalization (HE), wavelet-based regularization (Xiang et al. [10]), nonlinear smoothing and sharpening (Tanaka et al. [11]) and guided image filtering (GF) (He et al. [12]) in Fig. 7 to validate its effectiveness.

As can be observed, HE results in excessively bright enhanced images in Fig. 7(b) due to its dependence on the frequency of gray level values. In addition, some false contours are visible around the image edges in Fig. 7(b1), and the rich texture in the wall behind the porcelain wares in Fig. 7(b3) cannot be effectively enhanced. On the other hand, the approach proposed by Xiang et.al. cannot effectively enhance the texture detail in smooth areas, resulting in blurred patterns on the bed sheet (Fig. 7(c2)) and table linen (Fig. 7(c4)), in spite of its improvement in enhancing sharp edges. For the approach in [11], it is observed that some noise is present as shown in Fig. 7(d3), due to its adoption of a simple unsharp mask operation. While GF [12] avoids the problem of "gradient reversal", it mainly focuses on global enhancement, and does not adequately consider the complexity of local regions, leading to the deterioration of local rich texture patterns. It can be seen that the texture distribution on the cat's face (see Fig. 7(e1)), and the patterns on the table linen (see Fig. 7(e4)) have been changed to different degrees.

Fig. 8 shows the enlarged local texture regions highlighted in red in Fig. 7. It can be observed that the enhancement quality for lines or texture in smooth areas such as wrinkles in the cat's ear (see Fig. 8(a)), folds on the baby's clothes (see Fig. 8(b)), and patterns on porcelain wares (see Fig. 8(c)) are superior to others.

Table 2 summarizes the evaluation results for the different methods. It can be seen that the values of AG based on our approach are higher than those of other methods, which demonstrates its advantage in enhancing texture details. This is also reflected in the high AE values, which measures the capability of the approach in preserving texture information. Our result also performs well in resisting noise based on the comparison of the APSNR values.

In summary, the proposed algorithm can effectively preserve texture details. It is also capable of adapting to the degree of local texture complexity by creating sub-pixels and selecting the suitable fractional order.

3.3.2. Applications in medical image enhancement

Most medical images contain important structures, which are characterized by low natural contrast when compared to surrounding structures. To obtain high contrast directly from the imaging device is expensive in terms of acquisition time, and in general not preferable in view of the increased X-ray dose to the patient. Therefore, digital post-processing plays a vital role in medical image analysis. The proposed algorithm also performs well in medical image enhancement, and Fig. 9 compares the enhancement results of our approach with those of two previous methods for a chest X-ray image.

The method proposed by Setty et al. [13] applied multiscale retinex theory to improve the medical image as shown in Fig. 9(b). However, the resulting intensity saturation contributes to local texture information loss around the chest skeleton. Van Rikxoot et al. [14] focused on the detection of complex structures through constructing an effective classifier. However, the performance depends on a large number of
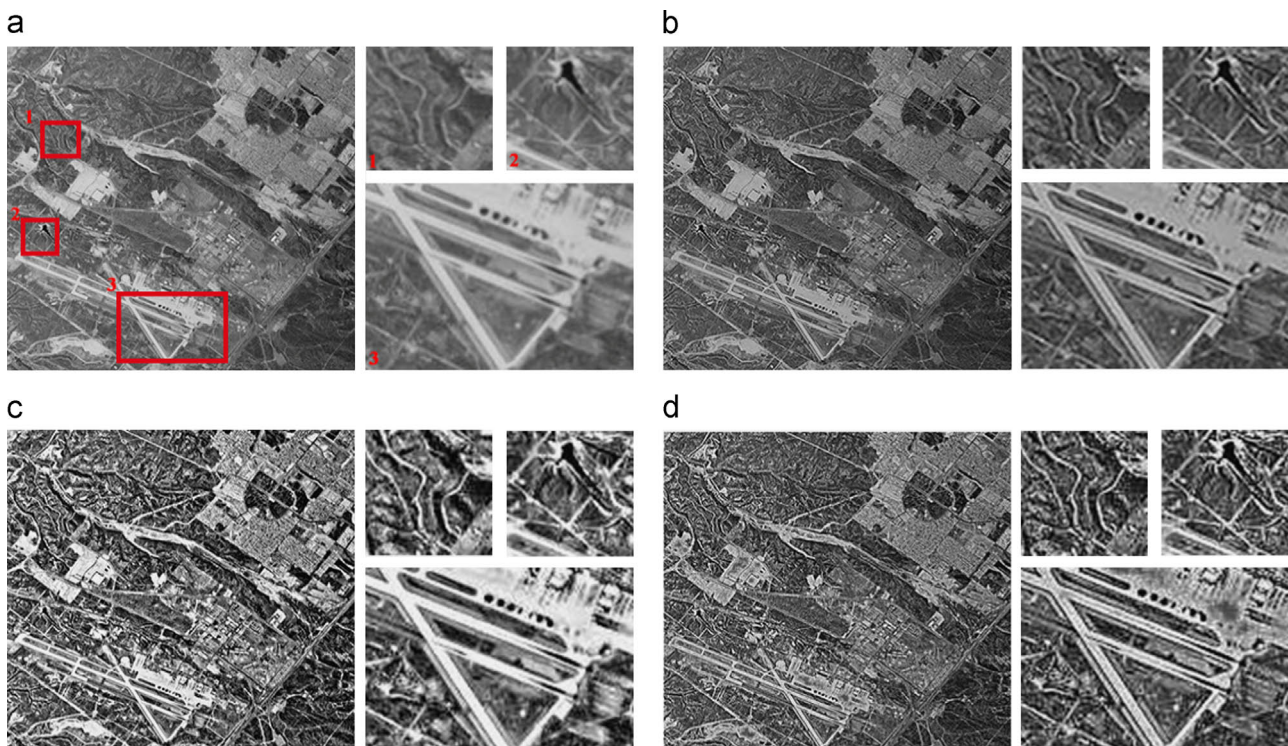

Fig. 11. Enhancement results of remote sensing image: (a) original, (b) Lee's result, (c) GF, and (d) our result. Three local regions highlighted in red are enlarged and placed at the right of each image. (For interpretation of the references to color in this figure legend, the reader is referred to the web version of this article.)
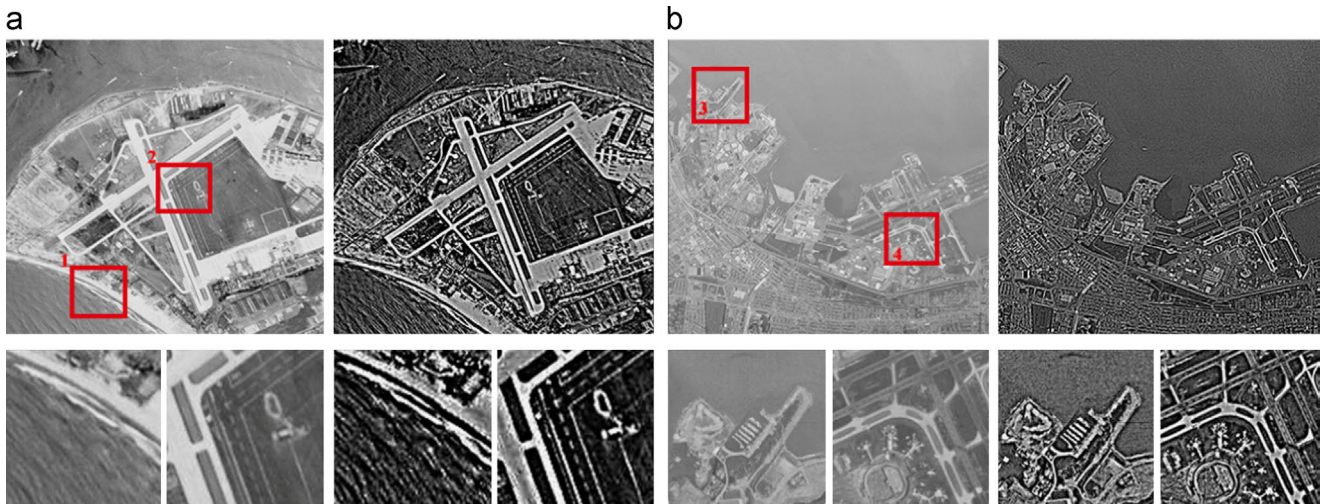
Fig. 12. Other remote sensing image enhancement results (left: original, right: our result).

training examples. Compared with these results, our approach has better image enhancement capability. This can be seen from the better resolved shoulder joint and rib cage in Fig. 9(e) (enlarged versions are shown in Fig. 9(f) and (g)). In addition, due to the newly proposed non-regular support region in Section 2.1, noise amplification can be effectively avoided before the application of the fractional differential operator. As a result, APSNR of our approach is higher than those of others, as seen in Fig. 9(i). We have also applied our approach to other X-ray/medical images from the benchmark set,[1] as shown in Fig. 10. These results demonstrate that our algorithm performs well in texture preservation and enhancement in smooth areas.

3.3.3. Application in remote sensing image enhancement

Remote sensing techniques are widely used for environmental protection, terrain mapping and military surveillance. However, different factors such as sensor limitation and atmospheric disturbance may lead to unsatisfactory imaging quality such as low contrast and/or blurring, which will in turn impede effective analysis. Therefore, enhancement of remote sensing images has become an important problem to be addressed. To show the capability of our approach in remote sensing image enhancement, we compare our result with those of Lee et al. [15] and GF [12] in Fig. 11.

Due to the adaptive intensity transformation adopted in [15], the winding river and highway in Fig. 11(b) appear more distinct, but other details are less discernible due to the overall low intensity of the image. On the contrary, due to overestimation of the pixel values in the GF case (see Fig. 11(c)), some regions like the roofs of buildings appear excessively bright. Fig. 11(d) shows our result. We can observe that our approach can take full consideration of local texture varieties, and details around the rivers or highways are more conspicuous than those of other methods. In addition, the overall intensity of the enhanced image is neither too high nor too low.

Other high resolution images from the dataset[2] are selected to validate the performance of our approach further, as seen in Fig. 12. It can be observed that the texture that is not usually well distinguished in smooth area, like ripple on the sea, is more discernible after enhancement through our approach.

4. Conclusion

In this paper, we have proposed an adaptive fractional differential operator mask for image enhancement. Through the identification of the main limitations of the previous fractional derivative-based methods, we obtain better performance by introducing a non-regular support region, and adaptively determining the associated fractional order such that the high degree of self-similarity in most images could be judiciously taken into consideration. In view of the capability of our proposed approach in enhancing important details of a large variety of image types, we shall further apply the algorithm as a pre-processing step to different areas such as object recognition and biometric analysis.

Acknowledgment

References

[1] L.I. Ying, H.U. Jie, Y.U. Jia, Automatic SAR image enhancment based on nonsubsampled contourlet transform and memetic algorithm, Neurocomputing 134 (2014) 70–78.

[2] C.H. Lee, H.G. Ha, W.K. Wang, Image contrast enhancement using classified virtual exposure image fusion, IEEE Trans. Consum. Electron. 58 (4) (2012) 1253–1261.

[3] Y.F. Pu, W.X. Wang, J.L. Zhou, Y.Y. Wang, H.D. Jia, Fractional order differentiation for digital image edge detection and realization of fractional order differential filter, Sci. China Ser. E: Inf. Sci. 38 (12) (2008) 2252–2272.

[4] A. Rocco, B. West, Fractional calculus and the evolution of fractal phenomena, Phys. A: Stat. Mechan. Appl. 265 (3) (1999) 535–546.

[5] Y.F. Pu, J.L. Zhou, X. Yuan, Fractional differential mask: a fractional differential-based approach for multiscale texture enhancement, IEEE Trans. Image Process. 19 (2) (2010) 491–511.

[6] C.B. Gao, J.L. Zhou, Image enhancement based on quaternion fractional directional differentiation, ACTA Autom. Sin. 37 (2) (2011) 150–159.

---

[1] ⟨http://peipa.essex.ac.uk/benchmark/databases⟩.
[2] ⟨http://sipi.usc.edu/database/⟩.

 [7] K. Zhang, J.B. Lu, G. Lafruit, Cross-based local stereo matching using orthogonal integral images, IEEE Trans. Circuits Syst. Video Technol. 19 (7) (2009) 1073–1079.
 [8] C.H. Oci, N.A. Iss, Adaptive contrast enhancement methods with brightness preserving, IEEE Trans. Consum. Electron. 56 (4) (2010) 2543–2551.
 [9] S.D. Chen, A new image quality measure for assessment of histogram, equalization-based contrast enhancement, Digit. Signal Process. 22 (4) (2012) 640–647.
[10] Z.J. Xiang, P.J. Ramadge, Edge-preserving image regularization based on morphological wavelets and dyadic trees, IEEE Trans. Image Process. 21 (4) (2012) 1548–1560.
[11] G. Tanaka, N. Suetake, E. Uchino, Image enhancement based on nonlinear smoothing and sharpening for noisy images, J. Adv. Comput. Intell. Intell. Inf. 14 (2) (2010) 200–207.
[12] K.M. He, J. Sun, X.O. Tang, Guided image filtering, IEEE Trans. PAMI 35 (6) (2013) 1397–1409.
[13] S. Setty, N.K. Srinath, M.C. Hanumantharaju, Development of multiscale retinex algorithm for medical image enhancement based on multi-rate sampling, in: Proceedings of the International Conference on Signal Processing Image Processing & Pattern Recognition, 2013, pp. 145–150.
[14] E.M. Van Rikxoort, B. van Ginneken, M. Klik, Supervised enhancement filters: application to fissure detection in chest CT scans, IEEE Trans. Med. Imaging 27 (1) (2008) 1–10.
[15] E. Lee, S. Kim, W. Kang, Contrast enhancement using dominant brightness level analysis and adaptive intensity transformation for remote sensing images, IEEE Geosci. Remote Sens. Lett. 10 (1) (2013) 62–66.

Maoxin Si received his B.S. degree in applied math from Xinjiang Agricultural University, Xinjiang, China, in 1982. He is an associate professor in computer science at Suzhou Vocational University. His research interests include image processing and algorithm optimization.


Shaohui Si received his B.S. degree in electronic and information engineering from Suzhou University of Science and Technology, Suzhou, China, in 2012. He is currently pursuing his M.S. degree in Suzhou University of Science and Technology. His interests include image enhancement, and fractional derivative theory.

Fuyuan Hu was a postdoctoral researcher at Vrije Universiteit Brussel,Belgium, a Ph.D. student at Northwestern Polytechnical University, and a visiting Ph.D. student at the City University of Hong Kong. He is an associate professor in computer vision and machine learning at Suzhou University of Science and Technology. His research interests include graphical models, structured learning, and tracking.

Baochuan Fu received his M.S. degree in electronic measurement and instrumentation from Harbin University of Science and Technology, Harbin, China, in 1988 and Ph.D. degree in control theory and control engineering from Tongji University, Shanghai, China, in 2008. He is a professor in computer science at Suzhou University of Science and Technology. His research interests include cybernetics and system optimization.
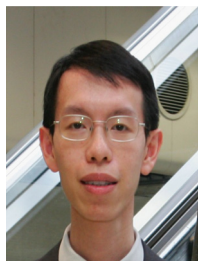
Hau San Wong received the B.S. and M.Phil. degrees in Electronic Engineering from the Chinese University of Hong Kong, and the Ph.D. degree in Electrical and Information Engineering from the University of Sydney. He is an associate professor in the Department of Computer Science, City University of Hong Kong. His research interests include multimedia signal processing, neural networks and evolutionary computation.

Heng Luo received his M.S. degree from Tongji University, Shanghai, China, in 2007 and his Ph.D. degree from University of Edinburgh, UK, in 2012 both in telecommunication engineering. His current research interests include information processing and system optimization.